Hindawi
Shock and Vibration
Volume 2021, Article ID 5566874, 14 pages
https://doi.org/10.1155/2021/5566874

Research Article

Seismic Response Analysis and Evaluation of Laminated Rubber Bearing Supported Bridge Based on the Artificial Neural Network

Bingzhe Zhang,[1] **Kehai Wang**,[1,2] **Guanya Lu**,[1] **and Weizuo Guo**[1]

[1]*School of Transportation, Southeast University, Nanjing, Jiangsu, China*
[2]*Research Institute of Highway, Ministry of Transport, Beijing, China*

Correspondence should be addressed to Kehai Wang; kh.wang@rioh.cn

Received 22 February 2021; Revised 6 April 2021; Accepted 16 April 2021; Published 26 April 2021

Academic Editor: Selçuk Erkaya

Laminated rubber bearings are commonly adopted in small-to-medium span highway bridges in earthquake-prone areas. The accurate establishment of the mechanical model of laminated rubber bearings is one of most critical steps for the bridge seismic response analysis. A new constitutive model of bearing based on the artificial neural network (ANN) technique is established through the static cyclic test of laminated rubber bearings, considering the bearing initial stiffness, friction coefficient, and other parameters such as the bearing sectional area, height, loading velocity, vertical load, and aging time. Combined with the ANN method, the ANN-based bridge seismic demand model is built and applied to the rapid evaluation of the bridge seismic damage. The importance of the bearing affecting design factors in the bridge seismic demands are ranked. The results demonstrated that the dimensions of the bearing and vertical load are the main factors affecting the bearings constitutive model. Based on the partial dependency analysis with the ANN-based bridge seismic demand model, it is concluded that the height of bearing is the key design parameter which affects the bridge seismic response the most. The ANN seismic demands model can fit the complex function relationship between various factors and bridge seismic response with high precision, so as to achieve the rapid evaluation of bridge seismic damage.

1. Introduction

LRBs (laminated rubber bearings) technique, as a prevailing and efficient seismic mitigation technique, is commonly employed in small-to-medium span bridges constructed in countries having the active seismic zones such as USA, Mexico, Japan, and China. As an important part of the seismic isolation system, LRB can effectively support loads and accommodate motions in different directions including vertical and shear displacements to protect the structure and surrounding infrastructure [1, 2]. Through the engineering investigation after the Wenchuan earthquake which happened in 2008 in Sichuan, China, the occurrence of plastic hinge and plastic damage in simply supported beam bridges with LRBs is much lower than in bridges with fixed bearings [3–5], and similar circumstances have been observed in the Northridge earthquake and the Chi-Chi earthquake as well [6]. An exemplar comparison of earthquake damage on bridges with steel bearing and those with LRB is shown in Figure 1; the piers of Hanwang bridge, which was using steel bearing, experienced serious plastic hinge damages during the Wenchuan earthquake, to reinforce and reuse the bridge which was not economical. Meanwhile, the seismic damage of Huilan bridge included bearings sliding away and shifting, with negligible damage in piers. After the minor repairs and reinforcements, traffic was quickly resumed. It was found that the LRBs play a critical role on the bridge seismic response and damage evaluation. Establishing a reasonable constitutive model of bearing was the prerequisite for analyzing the bridge seismic response accurately. At present, there is no multi-affection LRBs analysis model based on machine learning [7–10], so it is necessary to establish an accurate constitutive model based on the LRBs test datasets, further, to simulate and predict earthquake response of LRBs supported bridges.

In recent years, many studies based on the seismic response of bridges with LRBs have been conducted all over the world. The California DOT and Illinois DOT analyzed

(a) (b)

Figure 1: Typical earthquake damages on bridges supported by different types of bearings. (a) Mianzhu Huilan bridge (LRB). (b) Mianzhu Hanwang bridge (steel bearing).

the key design factors which affect the seismic performance of LRBs supported bridge, and the conclusion revealed that seismic motion intensity, pier height, and bearing type are the keys which affect the isolation system performance [11, 12]. Deng et al. and Billah et al. compared the impact of geometric parameters of the bearing and vertical load on the bridge seismic response by using FEM (finite element method) to model the rubber bearing supported bridge [13, 14]. Mitoulis et al. studied the influence on the characteristics of steel plate on the performance of rubber bearing under the combined effects of shear, rotation, and axial load [15, 16]. Xiang et al. investigated the shear and sliding behaviors of rubber bearing with different vertical loads and concluded that the sliding friction coefficient of the bearing was inversely proportional to the vertical load and was ranged between 0.11 and 0.57 [17]. Wu et al. proposed a trilinear mechanical model based on a series of quasistatic tests of LRBs [18]. Bhuiyan et al. established a speed-dependent mechanical model based on the test data [19]. Compared with the abovementioned studies, there are bearing constitutive models of mechanical experimental and finite element method, but the samples of bearings in other research studies are less in quantity, and the distribution has limitations. And several regression methods have been used in fitting the mechanical behavior of the test of rubber bearing, such as linear regression and exponential regression, but the ANN technique which is the nonparametric model has the ability to simulate the complex constitutive model of the bearing with high accuracy. Although these studies took into account one or several factors on the performance of LRBs, such as vertical load, loading speed, and geometry, the LRBs mechanical model integrating multiple factors simultaneously is not yet established, and the uncertainty analysis of the parameters of bearing has not been evaluated previously.

The booming machine learning (ML) technologies have been proven to be a successful classification and prediction tool in some traditional engineering applications. Some successful adoptions of ML in multifactor seismic response analysis of bridges have been published recently. Ghosh et al. and Guo et al. used linear models and ANN models to establish seismic response models for cable-stayed bridges and small-to-medium span bridges [20, 21]. Jia et al. solved a ranking problem of the importance of structure type, bearing type, and other 9 features based on the random forest model using the datasets collected during Wenchuan earthquake damage investigations, and the artificial neural network model is adopted to predict the earthquake damage of bridges [22]. Hwang et al. and Kiani et al. implemented certain algorithms such as the k-nearest neighbor, simple Bayes, random forest, and decision tree to analyze and predict the seismic response, and it was concluded that the dataset is the key to the learning performance, and accuracy of the classification models was better than those of the regression models in seismic response prediction [23, 24]. Figueiredo et al. explored a hybrid approach for damage detection with machine learning techniques [25]. Wang et al. and Alwanas et al. proposed a methodology which employs the machine learning methods to establish the constitutive models of structural member by using the test data [26–29]. The above research studies' progress shows that the ML can effectively fit the complex functioning relationship in seismic response analysis, but yet, it is not seen to discuss and order the effect of the bearing geometric parameters and non-geometric parameters on the bridge seismic demands by using ANN technique.

It is necessary to establish a reasonable constitutive model of the bearing which is the foundation for analysis of the bridge seismic response and evaluating the seismic damage. The constitutive model of LRBs in the Chinese specification only considers the influence of geometry on the initial stiffness of bearing [9, 10] but does not considers other factors such as vertical load, aging time, and loading speed. The ANN method can effectively simulate the mechanical constitutive model of rubber bearing integrating multiple factors with high accuracy and fit the complex functioning relationship in seismic response analysis. A laboratory shear testing program of LRBs is proposed in this study. Based on the experimental results and the ANN method, a constitutive model is developed to accurately fit the bearing mechanical

constitution. A large-scale nonlinear seismic analysis is carried out on a typical three-span continuous bridge, and a seismic demands model is established through the ANN to evaluate the seismic damage. In addition, by analyzing the partial dependence relationship of the bearing design parameters and seismic demands model, the order of affecting the bearing design parameters on the bridge seismic response is determined.

2. Test Procedures

2.1. Specimen Preparation. In this study, the behavior of eight circular laminated rubber bearings with 370 mm diameters, with full-scale bearings commonly used at T-girder small and medium bridges, is investigated. The laminated rubber bearings without thick end plates are covered by rubber material. The structure diagram of bearing is shown in Figure 2, and the bearing conformation and material mechanics parameters satisfied the design specifications of highway bridge elastic bearing of China (MOTC) [10].

The test specimens consisted of two batch of LRBs; the first batch specimens are the new LRBs, and the relevant research conclusions can be found in [18, 30]; the second batch specimens are the batch one specimens after four years of natural atmospheric aging. Load the weight on the bearing during the aging time to ensure that it conforms to the normal load state. Then, the actuator exerted cyclic horizontal displacement to the bottom steel plate of the bearing. The parameters for vertical load, loading velocity, rubber material, and aging time of the testing program form are given in Table 1.

2.2. Test Procedure. The LRBs quasistatic shear testing was carried out in the Experimental Lab of Hengshui China Railway Construction Engineering Rubber Co., Ltd. The setting up of the experimental device shown in Figure 3 included 30,000 kN capacity of the coordinated loading system. The example specimen of bearing that was placed between the top and the bottom steel plates is shown in Figure 3. The steel plate was kept smooth to ensure that sliding response will take place between the bearing and steel pad. There were no constraint components to set in the pad surface for simulating the true state of the bridge bearing placement.

First, the dead load was implemented on the bearing specimens through a vertical servo actuator. Second, the dead load is maintained at the given value by the vertical servo actuator automatically adjusted, ignoring the bearing horizontal deformation. Finally, the target shear circular horizontal displacement is applied to the bottom supporting plate by the horizontal executor. The equivalent shear strain (ESS) is adopted as the loading displacement measurement, in which the test program has set a target of 400% ESS as shown in Figure 4 [17]. The horizontal and vertical executors operate independently as they are controlled by two separate hydraulic systems. Record the bearing's horizontal force-replacement curve during the test. The loaded displacements included the bearing shear deformation and the sliding

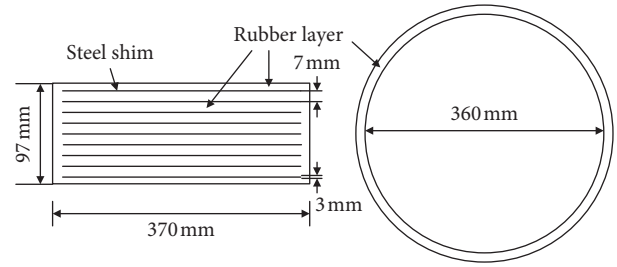

Figure 2: Configuration details of the bearing specimens.

displacement. Each steel plate is marked with a 5 cm × 5 cm white gird and specimen profile on the supporting surface for more accurate measurements of the sliding displacement. The vertical white lines are carried out on the side of the bearing to measure the extent of the warped during the testing.

3. Test Results and the LRB Mechanical Model

3.1. Bearing Response. As the vertical pressure of laminated rubber bearings is preserved on the target value, the horizontal displacement of the bearings increased gradually. The deformation of the bearing is observed (Figure 5). There are three stages during the loading process, which represent different characteristics of the displacement response, and each stage is as follows:

Stage I (ESS <75%). The increasing displacement demands of the test are from the pure shear deformation in the elastomer layer rather a sliding response. The force-displacement relationship is basically linear.

Stage II (75%< ESS <100%). With the increasing of horizontal actuator displacement loading, the shear deformation of the rubber layer of specimen continued to increase as well. At the same time, the differences from Stage I that slight sliding displacement and warping are observed at the bearing interface. The initial stiffness begins to decrease, and an inflection point of the line is observed from the force-displacement curve. At this stage, the bearing sliding response and elastic shear deformation constitute the bearing recorded displacement by the horizontal actuator.

Stage III (ESS >100%). The bearing performed the sliding response almost, and the ratio of shear deformation and warping are no longer rising in this stage. The horizontal force is equal to the friction force during the sliding response approximately. As the number of loading circle increases, a large amount of rubber clastic appears between the steel plate surfaces and bearings. Sliding displacement increases at a high rate, resulting in an increase in the amount of displacement imposed. Satisfactorily, the LRBs did not occur as delamination and instability between the steel plate and the rubber layer during the test, and the mechanical properties are stable even under the seismic demands of long distance.

In this study, the sliding LRB constitutive model is developed with the bilinear elastic-plastic model, which is

Table 1: Testing plan.

Test specimen	Vertical load (MPa)	Loading velocity (mm/s)	Rubber material	Research parameters	Aging time (years)
Y1-8-30-N	8	30	Neoprene material	Loading velocity	0
Y1-8-3-N		3			0
Y1-8-45-N		45			0
Y1-4-30-N	4	30		Vertical load	0
Y1-6-30-N	6	30			0
Y2-8-30-N	8	30	Natural rubber	Rubber material and loading velocity	0
Y2-8-3-N		3			0
Y2-8-45-N		45			0
Y1-8-30-A	8	30	Neoprene material	Loading velocity	3.5
Y1-8-3-A		3			3.5
Y1-8-45-A		45			3.5
Y1-4-30-A	4	30		Vertical load	3.5
Y1-6-30-A	6	30			3.5
Y2-8-30-A	8	30	Natural rubber	Rubber material and loading velocity	3.5
Y2-8-3-A		3			3.5
Y2-8-45-A		45			3.5

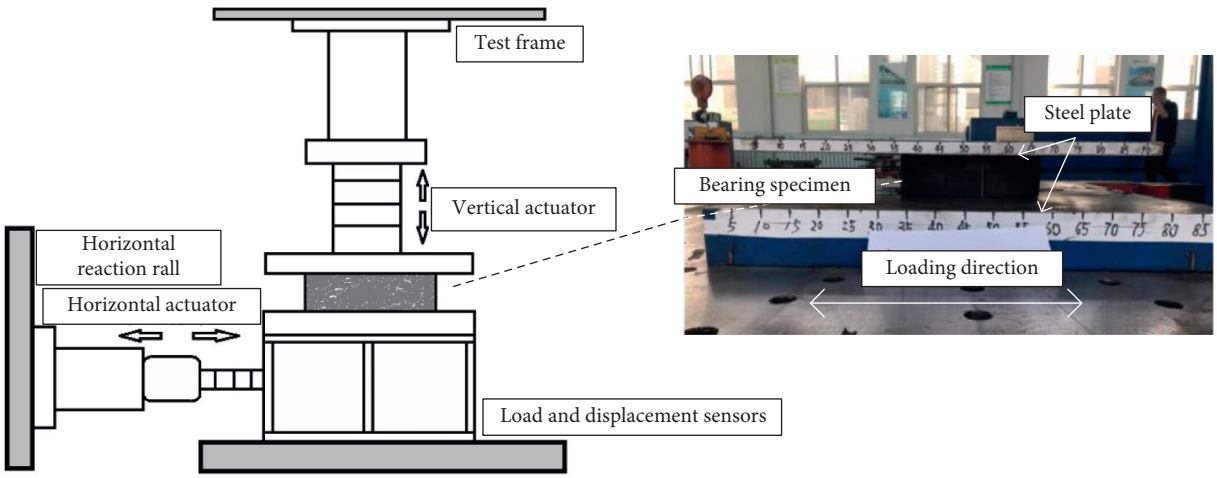

Figure 3: Testing setup.

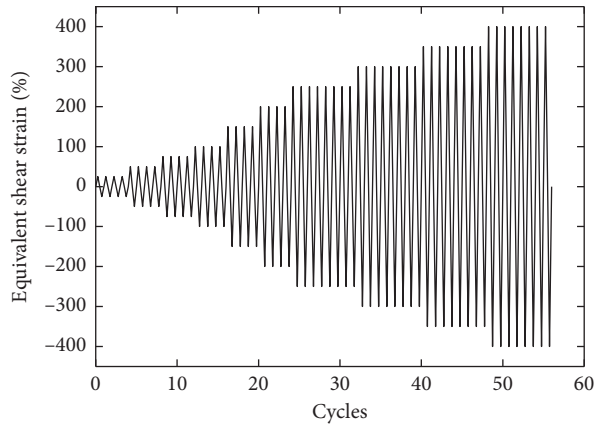

Figure 4: Cycle loading testing protocol.

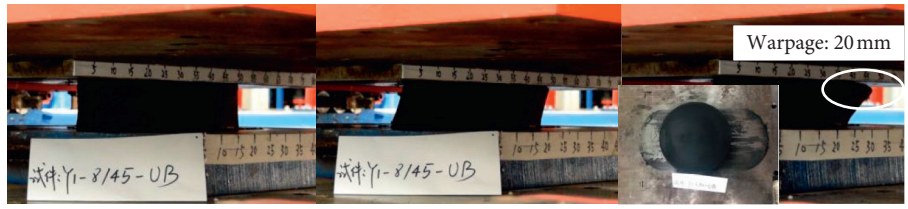

Figure 5: Bearing response in different stages.

defined by two parameters: sliding friction coefficient (μ) and initial shear stiffness (K_e). It is supposed that the displacement response behavior of LRB is divided into elastic response stage and sliding response stage; the first stage is the elastic behavior before sliding (Stage I), corresponding to the first red line of Figure 6, which is characterized by initial shear stiffness (K_e) mainly. When the horizontal loading is larger than the maximum friction force ($F_{\max}$) of the bearing (Stage III), the plastic deformation will be developed, corresponding to the horizontal red line in Figure 6. According to Coulomb's friction criteria, after the sliding resistance is reached, the maximum friction force ($F_{\max}$) is characterized by the sliding friction coefficient (μ). The sliding LRB model is computed by the following formula.

When $x \le x_1$,

$$F = K_e x. \tag{1}$$

When $x > x_1$,

$$F = F_{\max} = \mu N, \tag{2}$$

where $x_1 = F_{\max}/K_e$.

Based on the experimental results, the sliding friction coefficient (μ) is developed. The sliding friction under different vertical loads is analyzed (Figure 7). When the vertical loads are 4 MPa, 6 MPa, and 8 MPa, the surface friction coefficients of LRB are 0.42, 0.26, and 0.2, respectively. It can be concluded that the vertical load negatively correlates to the friction coefficient. The reason for this change in friction coefficient is with the sliding of bearing generates heat, and the rubber of the contact surface melts and adheres to the steel plate, which changes the friction coefficient of the steel plate surface. Therefore, investigating the friction sliding characteristics and laws of the LRB under vertical earthquake and the influence on the structural dynamic response is necessary.

3.2. Bearing Analytical Model Based on the ANN. In this study, 140 sets of LRB force-displacement curves data of foreign scholars were collected [31–34]. The parameters of bearing such as the sectional area (A), height (H), loading velocity (V), vertical load (L), and aging time (T) were counted, which maintain the range of the 30 m span highway bridge bearings in Table 2. The peak point of displacement (blue dot in Figure 6) in each cyclic curve is found by Matlab software; the initial stiffness (K_e) and coefficient of friction (μ) of the bilinear model are determined. The data preprocessing of the above parameters is normalized to reduce the influence of data units.

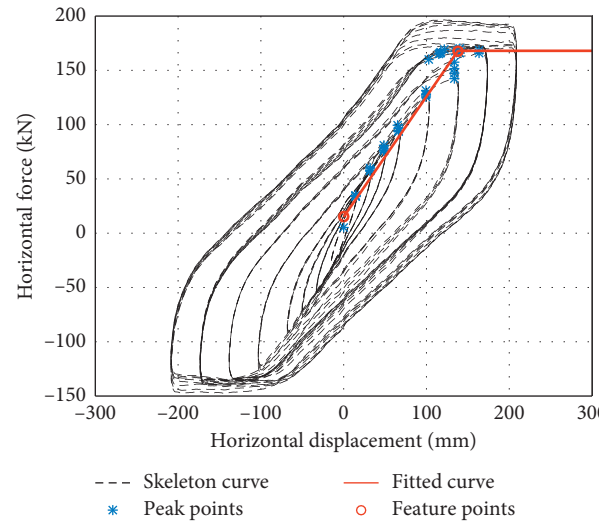

Figure 6: Specimen Y1-8-45 force-displacement curve.

Controlling the number of input variables optimizes the structure of the neural network, and more input variables may be redundant. So, it is necessary to analyze the correlation of the research data and determine the key design parameters that affect the bearing mechanics performance.

The parameters of A, H, V, L, and T are used as the input variables, and the K_e and μ are used as the output variables. First, the correlation analysis is performed on the input variables, and the correlation matrix is shown in Figure 8. The results show that the sectional area and height have a certain correlation with loading velocity, and the correlation coefficients are 0.85 and 0.47, respectively, so the loading velocity cannot be used as an independent variable. In addition, the correlation analysis is performed of input and output variables too. The result shows that the initial stiffness is obviously related to the sectional area and height, and the correlation coefficients are 0.45 and −0.56, respectively. The friction coefficient is obviously related to the vertical load, the correlation coefficient is −0.83, but the correlation with other parameters is not strong. The conclusion conforms to Huang's research results [35, 36]. Therefore, sectional area (A), height (H), and vertical load (L) are determined as independent input variables.

There are numerous factors affecting the seismic response of bearing and containing a large number of nonlinear processes. It is difficult to simulate the relationship accurately by the linear regression model, but it can be achieved by the nonparameter model such as the ANN with high precision. The ANN calculates the gradient term g_j of

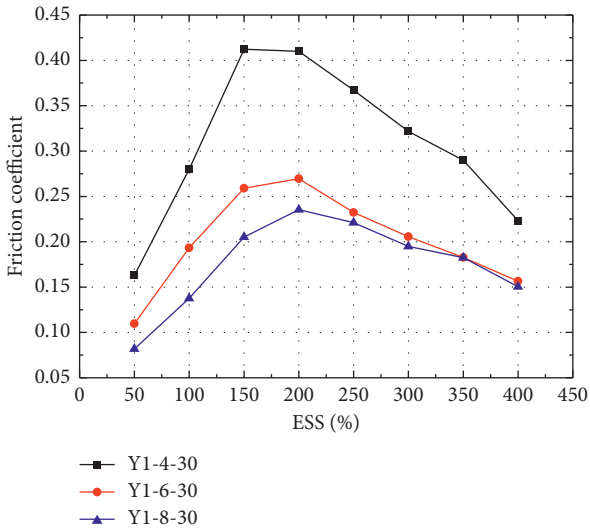

Figure 7: Observed friction (μ) versus ESS.

Table 2: The distribution of bearing parameters.

Factor	Range maximum	Range minimum
A (m)	0.36	0.07065
H (m)	0.204	0.048
V (m/s)	0.835	0.003
L (MN/m)	10	1.5
T (year)	20	0

the output layer neurons and the gradient term e_h of the hidden layer neurons, with the average variance E_k minimum of the network at (x_k, y_k) as the target.

$$E_k = \frac{1}{2}\sum_{j=1}^{l}\left(\hat{y}_j^k - y_j^k\right)^2,$$

$$g_j = -\frac{\partial E_k}{\partial \hat{y}_j^k}\cdot\frac{\partial \hat{y}_j^k}{\partial \beta_j}, \tag{3}$$

$$e_h = -\frac{\partial E_k}{\partial b_h}\cdot\frac{\partial b_h}{\partial \alpha_h}.$$

In this study, the fitting of the LRB model is carried out by the ANN, and the control group is multivariable linear regression (MLR). Based on the Python computer programming language, the LRB mechanical model was developed by the multilayer perceptron regressor model and the linear regressor model, respectively. The ANN model consisted of several layers: an input layer and two hidden layers with 50 neurons in one hidden layer to ensure smooth decision boundary and an output layer. The inlayer and interlayer connections are implemented through activation functions. The fitted goodness R^2 is used as the evaluation index for the performance of the model. As the ANN is a nonparameter model, the LRB common types are extracted from the ANN model presented in Table 3.

The control group LRB constitutive model by MLR is expressed as

$$\begin{aligned} K_e &= 0.297A - 0.623H - 0.031L + 0.344, \\ \mu &= -0.056A - 0.106H - 0.602L + 0.707. \end{aligned} \tag{4}$$

The results demonstrate that R^2 of friction coefficient of the LRB model by the ANN method is 0.902, and R^2 of initial stiffness is 0.852. The R^2 of friction coefficient of the LRB model by the MLR method is 0.86, and R^2 of initial stiffness is 0.82. It can be concluded that the ANN method is better than the MLR method in fitting the LRB model.

By comparing the initial stiffness of the bearing, the K_e value of the ANN model is lower than the recommended value of the MOTC [9], such as the GYZ d400 × 54 model, and the value of the ANN model is 1342 kN m, which is much smaller than the recommended value of the MOTC; it is 3770 kN m. The maximum friction coefficient of the ANN model is 0.245, which decreases with the increase of vertical load, and the minimum is 0.09, which is different from the MOTC value of 0.2.

4. Seismic Response of LRB Bridge

4.1. Bridge Finite Element Modeling. A typical example was proposed to study and compare the effects of different LRB models on the seismic response demands of highway bridges. The typical prestressed concrete continuous bridge was located in the near-fault seismic area of Wenchuan province of China. The span was 90 m in total; one single span was 30 m long, consisted of 1.7 m high five T-girders with a total width of 10 m. The substructure was composed of a 10 m high double column constructed of C30 concrete with a circular cross-section of 1.5 m in diameter, as shown in Figure 9. The piers were reinforced longitudinal with HRB 400 rebar with a diameter of 28 mm, and the reinforcement rate was 1.5%. Circle steel bars with a diameter of 10 mm were used as hooping, each steel bar was spaced 100 mm apart, and the thickness of the covered layer of concrete was 50 mm. The girder was supported by one bearing at the bent top, where the type was GJZ400 × 400 × 69. The bearing in this model was subjected to the superstructure gravity loading, maintaining an average pressure of 5 MPa. For the regular service demands, five LRBs were placed in each span. The concrete shear keys were positioned to limit the horizontal displacement of the girder, in which the gap between the beam and shear keys was 0.05 m.

An integrated nonlinear finite element model was established in OpenSees software, which was considered as the diverse material performance. In this model, seismic masses of the structure are assumed to be lumped among the components. The beam, pier cap, and diaphragms are simulated by linear elastic beam elements for they will not be damaged in the earthquake. However, for the small and medium span bridges, the top and bottom of the piers often appeared as plastic hinge deformation, and nonlinear fiber elements were used for simulation. The circular pier section was divided into three parts, including reinforcement steel fibers, confined concrete fibers, and nonconstrained concrete fibers. The concrete area was simulated by the Concrete01 material, which was based on the Kent–Scott–Park

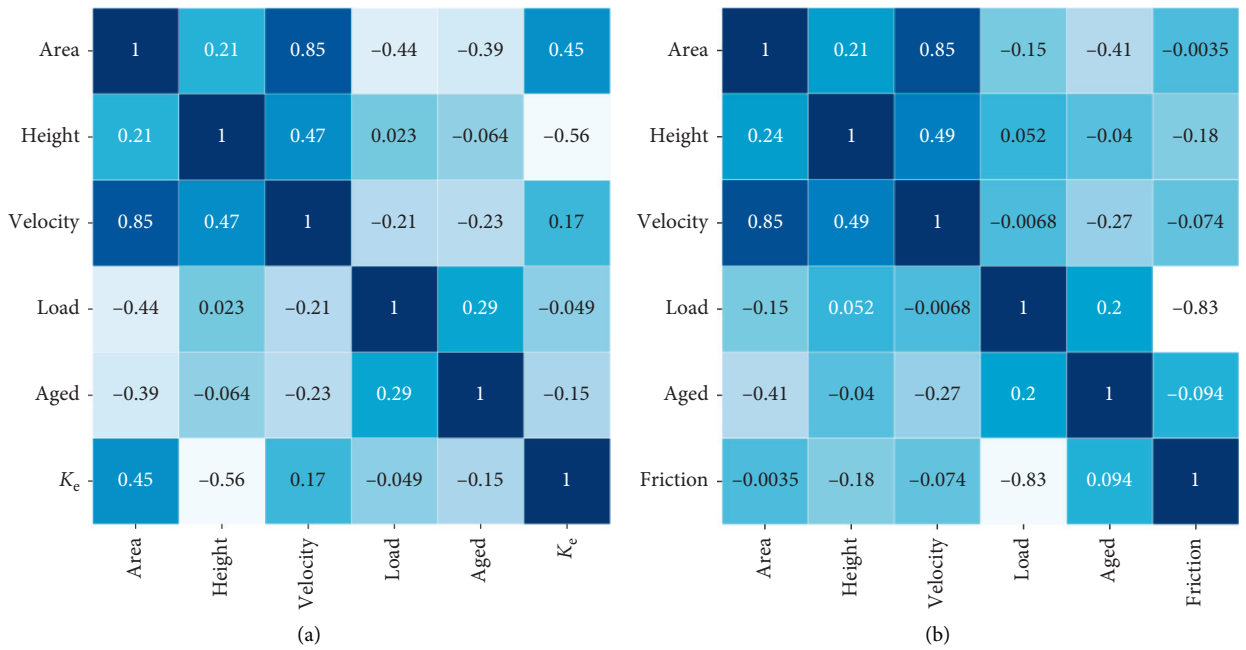

Figure 8: Correlation matrix for bearing parameters with (a) K_e and (b) μ.

Table 3: LRB model by the ANN.

A (m^2)	Type	H (mm)	K_e (MN/m)	μ				
				P_1	P_2	P_3	P_4	P_5
0.07065	d300	52	0.990	0.232	0.201	0.171	0.141	0.108
		63	0.894	0.227	0.195	0.165	0.135	0.102
		74	0.797	0.221	0.190	0.159	0.130	0.096
		85	0.700	0.215	0.184	0.154	0.124	0.090
0.09	300 × 300	52	1.121	0.234	0.203	0.173	0.142	0.110
		63	1.024	0.229	0.197	0.168	0.136	0.105
		74	0.927	0.223	0.192	0.162	0.131	0.099
		85	0.830	0.218	0.186	0.156	0.125	0.094
0.0962	d350	63	1.066	0.235	0.204	0.174	0.142	0.110
		74	0.969	0.229	0.198	0.168	0.137	0.105
		85	0.872	0.224	0.192	0.163	0.131	0.100
		96	0.775	0.219	0.187	0.158	0.125	0.094
0.1225	350 × 350	63	1.242	0.237	0.205	0.174	0.143	0.111
		74	1.146	0.231	0.199	0.168	0.137	0.105
		85	1.049	0.225	0.193	0.162	0.131	0.099
		96	0.952	0.219	0.187	0.156	0.125	0.093
0.1256	d400	54	1.342	0.237	0.206	0.174	0.143	0.112
		69	1.210	0.231	0.200	0.168	0.137	0.106
		84	1.079	0.225	0.194	0.162	0.131	0.100
		99	0.947	0.219	0.188	0.156	0.125	0.094
0.16	400 × 400	54	1.574	0.245	0.213	0.182	0.151	0.119
		69	1.442	0.237	0.205	0.174	0.142	0.111
		84	1.310	0.228	0.197	0.166	0.134	0.103
		99	1.178	0.220	0.189	0.157	0.126	0.095
0.1589	d450	69	1.435	0.236	0.205	0.174	0.142	0.111
		84	1.303	0.228	0.197	0.166	0.134	0.103
		99	1.171	0.220	0.189	0.157	0.126	0.095
		114	1.039	0.212	0.180	0.149	0.118	0.086
0.2025	450 × 450	69	1.728	0.240	0.209	0.177	0.146	0.114
		84	1.596	0.232	0.200	0.169	0.138	0.106
		99	1.465	0.223	0.192	0.161	0.129	0.098
		114	1.333	0.215	0.184	0.153	0.121	0.090

Note: P_i, vertical load. $P_1 = 5$ MPa; $P_2 = 6$ MPa; $P_3 = 7$ MPa; $P_4 = 8$ MPa; $P_5 = 9$ MPa.

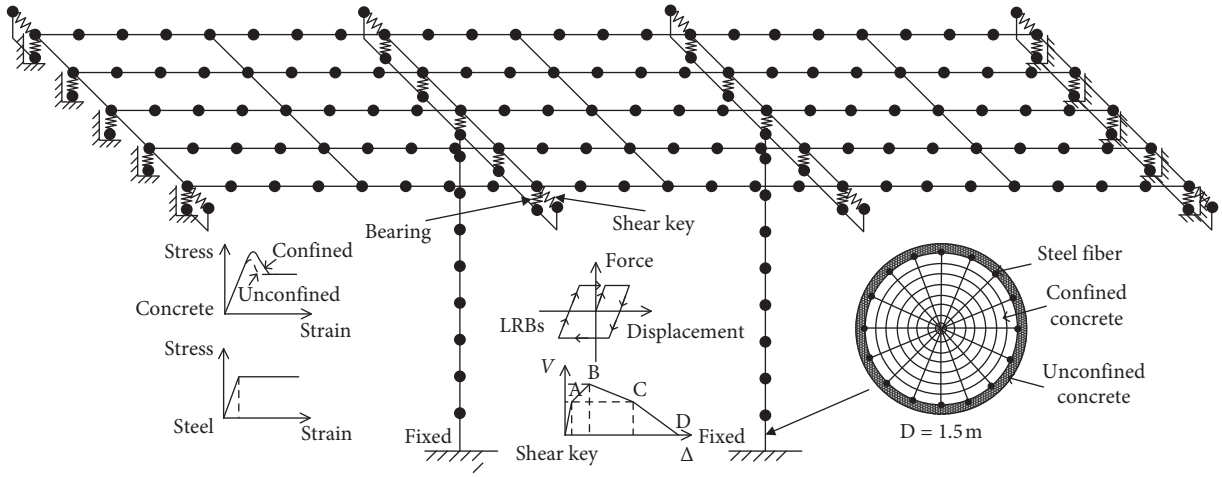

Figure 9: Finite element model of prototype bridge.

model [37], and the reinforced fibers were simulated by the Steel02 material accounting for the Bauschinger effect [38]. The sliding behavior of LRB was similar to the mechanical characteristic of Steel02 in OpenSees. The constitutive model of the LRB component was defined by the initial shear stiffness and the friction coefficient, which specifies the behavior of sliding on the steel plate.

The bridge seismic response may be influenced by the pounding effects of girders and shear keys, especially the high global motion intensity. In this study, a shear keys model consisting of two hysteretic elements was developed in OpenSees, which was taken into the contribution of concrete and steel. The pounding effect was matched by the connection of the gap element and shear keys, and the parameters of the model were determined by the material and geometric dimensions [39]. The interaction between soil and foundation was ignored in the whole bridge model, and fixed constraints on the column foundation were imposed.

4.2. Ground Motion Selection and Bearing Parameters Distribution. Vertical earthquake motion will increase the vertical load of the bearing and thus affect the coefficient friction. In this study, vertical earthquake intensity is selected as the index of the vertical load on the bearing, and the vertical seismic load of the bearing is assumed to be the maximum force response value under vertical earthquake movement. The 1994 Northridge earthquake is obtained from the PEER Ground Motion Database because it is the characteristic of near-fault ground motions. Table 4 provides the details of these two direction ground motions. The peak ground acceleration (PGA) is used as an indicator of seismic intensity measurement (IM) [9]. The PGA of the horizontal ground motions is scaled from 0.2 g to 0.8 g in increments of 0.1 g and input in the transverse direction. The ratio of the horizontal component to the vertical component is 157%, adjusted vertical ground motions at the same scale to ensure the integrity of the near-fault ground motion characteristics [40]. In addition, the setting of PGA-vertical to 0 adds to simulate none of the vertical components.

According to the normal used loading requirements and the design demand of the highway bridge, the basic design parameter is generated by possible values of the Latin hypercube sampling (LHS) simulation probability distribution function. The LHS is a hierarchical random process that provides an effective method for sampling from variable distribution [41]. In the independent variables $X_1, X_2, \ldots, X_k$, the LHS established a dataset of 2916 bearings design parameters with a 95% guarantee rate, by dividing each variable into N equal probability intervals and obtaining each variable paired with other variables randomly. The bearing parameters are divided into two categories to clearly express the effect of the bearing design parameters on the bridge seismic response. The sectional area (A) and height (H) are divided into the bearing geometry parameters; the earthquake vertical component (PGA-V) and the bearing number (B), which is bearing number of one span, are divided into the bearing nongeometric parameters. The ANN bearing models are introduced in Section 3.2 of getting the initial stiffness and coefficient of friction. Table 5 provides the distribution of 2916 bearings design parameters.

4.3. Comparison between Different Bearing Models. Three LRB analysis models were proposed to compare the effects of different bearing models on the seismic response of bridges, so as to determine the bearing key parameters that affect the seismic response of the small-to-medium spanning highway bridges. The models were as follows:

Model 1. An LRB analysis model based on the ANN was established, considering the influence of vertical earthquake component on the coefficient of friction

Model 2. An LRB analysis model based on MLR was established, considering the influence of vertical earthquake component on the coefficient of friction

Model 3. An LRB analysis model based on MOTC was established, regardless of the influence of vertical seismic motion on the friction coefficient, and the friction coefficient was a fixed value of 0.2.

Table 4: Ground motion.

Earthquake	Year	Station	Magnitude	PGA-horizontal (g)	PGA-vertical (g)	Rjb (km)	Rrup (km)
"Northridge-01"	1994	"Sylmar—OVM FF"	6.69	0.843	0.536	1.74	5.3

Table 5: Bearing parameters distribution.

Factor	Range maximum	Range minimum
A	0.36 m^2	0.1225 m^2
H	0.15 m	0.054 m
B	5	2
PGA-V	0	0.508 g
PGA-horizontal (PGA-H)	0.2 g	0.8 g

Considered that the seismic damages such as excessive displacement of bearing and plastic hinges in the pier were of the higher level of harmfulness, the displacement of the pier top in first span was selected as the pier seismic response indicator, and the bearing ESS was selected as the bearing response indicator, as shown in Figure 10.

Figure 10 describes the peak displacements of the bearing and pier under ground motion of three models. For the different model, considering that vertical seismic motion will greatly affect the seismic response of bridges. As the PGA increases, the displacement response of bearing and pier gradually increases. The displacement responses of bearing of the ANN model and MLR model are larger than the MOTC model; since the characteristics of the coefficient of friction with vertical load changes are accounted, the bearings are more prone to sliding which increases the bridge seismic response; thus, the pounding effect will greatly increase the seismic response of the bridge. For displacement response on the pier top, the result of the MOTC model is smaller than the ANN model and MMLR model when PGA $\leq$0.6 g. While at PGA >0.6 g, the pier displacement response of the MOTC model is much greater than the ANN model and MLR model, due to the friction of the MOTC model after the bearing sliding is higher than other two models.

4.4. Seismic Response Demands Analysis. In the traditional seismic demand analysis, only one single variable is considered each time, and the relative importance of the different bearing properties in the seismic demands model could not be determined. To amend such a deficiency, a seismic demand model using the ANN technique was proposed as depicted in the following steps:

Step 1: The input variables were sampled by the Latin hypercube sampling technique across the range of parameters. Then, 2916 statistically significant 3D bridge finite element models with different bearing parameters were built for the bridge nonlinear dynamic response analysis. After the nonlinear dynamic response analysis, the initial seismic demands samples were generated.

Step 2: The initial seismic demand samples were divided into a training dataset (75 percent) and a test dataset (25 percent). The training dataset was entered into the ANN regressor model for training.

Step 3: The connection rights and thresholds were randomly initialized in the network, calculating the output $\widehat{y}_k$ of the current sample

Step 4: By comparing the expected E_k and network output, the gradient g_j of the output layer and gradient e_h of the hidden layer were calculated (forward process)

Step 5: The ANN model within the expected error range was generated by continuously adjusting connection right ω_{hj}, υ_{ih}, and threshold θ_j, γ_h in calculation of the multilayer hidden layer

Step 6: The test dataset was entered into the ANN bridge seismic demands model to evaluate its performance and accuracy

Through the R^2 of the initial sample set and the output of the ANN demands model, the validity of the ANN seismic demand model was verified. The seismic damage criteria of the small-to-medium span highway bridge was introduced [30, 42], which were three levels of noninjury, minor injury, and serious injury, and three tags are defined as shown in Figure 11. The displacement of bearing and pier top are selected as the measurements of the bridge seismic demands. The ratio of accurate tag allocation number to total quantity is defined as the accuracy of the ANN model, indicating that the model has the capability to determine the bridge damage level accurately.

The results show that the R^2 of the bearing parameter and pier seismic demands in the ANN model was 0.985, and the R^2 of the bearing seismic demands is 0.978, which shows that the ANN method can predict the seismic demands with high precision. Figure 12 shows the comparison of damage distribution obtained by the ANN model results and those obtained from nonlinear dynamic analysis (NDA), with 98% accuracy of tag allocation (98/100), 2 errors in 46 green labels, and 2 errors in 34 red labels.

The partial dependence plots show the relationship between the ANN seismic demand model and bearing features of attention, downsizing other features to express the relative importance of each feature. It is appropriate to select a small size of feature datasets, generally choosed from the most important features. Thus, they are generally chosen among the most important features. Figures 13 and 14 show the dependences between the ANN seismic demand model and bearing geometry parameters, bearing nongeometry parameters.

From the Figure 13, it can be concluded that the original values of partial dependency function with bearing height to the seismic demands of pier and bearing are 22.59–28.32 and 1.42–2.89, which are greater than the values of the bearing area for 22.35–25.47 and 1.81–2.17. With the bearing's cross-sectional area (A) increased, the pier's seismic demands increased correspondingly, as shown in Figure 13(a). This observation is reasonable because the increase of the cross-

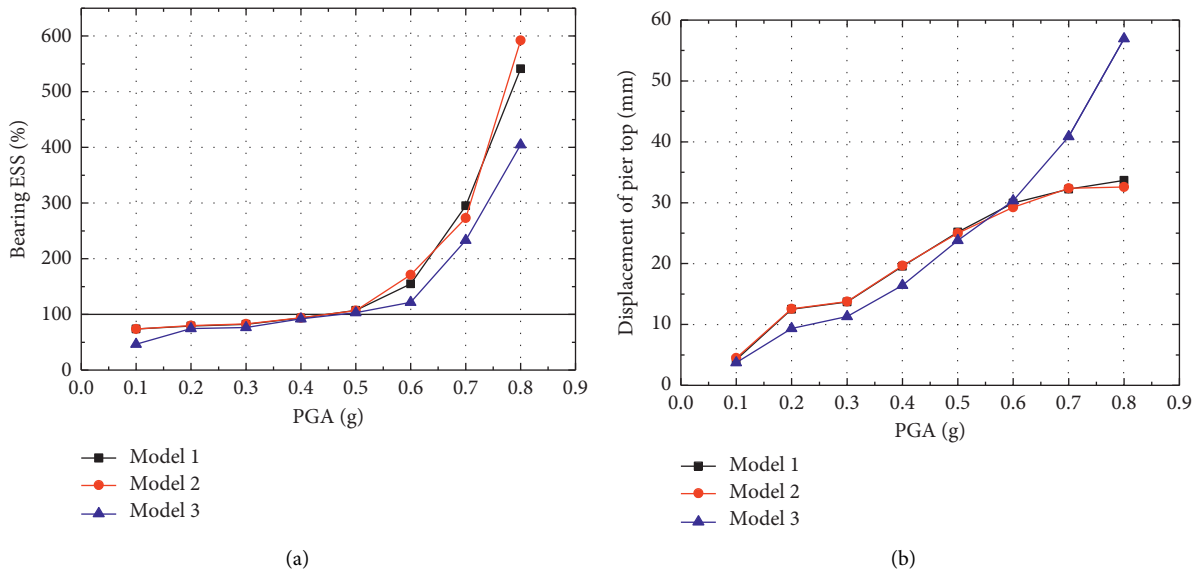

Figure 10: Comparison of (a) bearing equivalent shear strain and (b) pier displacement response using various bearing models.

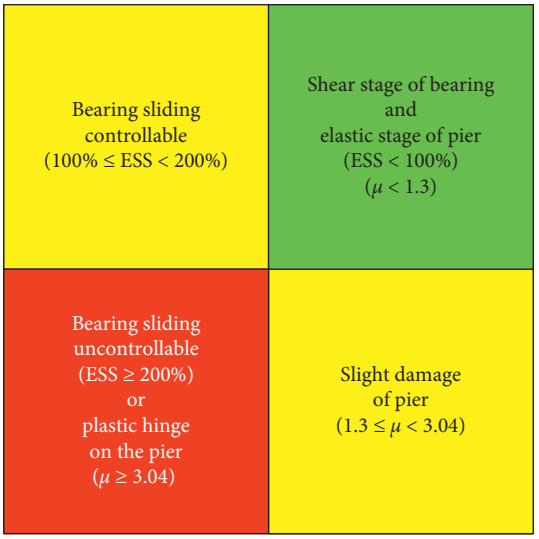

Figure 11: The seismic damage criteria of the bridge.

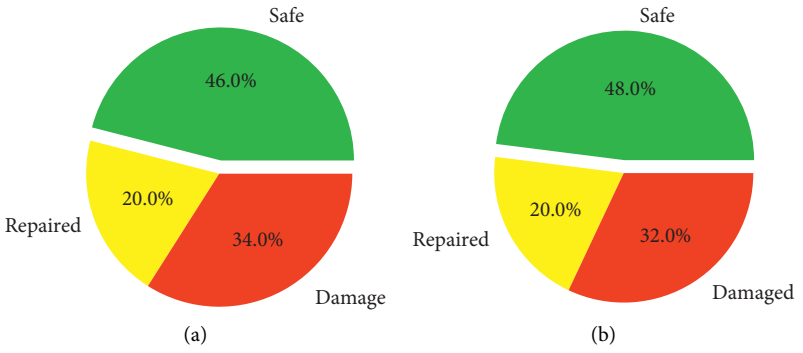

Figure 12: Damage distribution of the test dataset. (a) NDA results. (b) ANN model results.

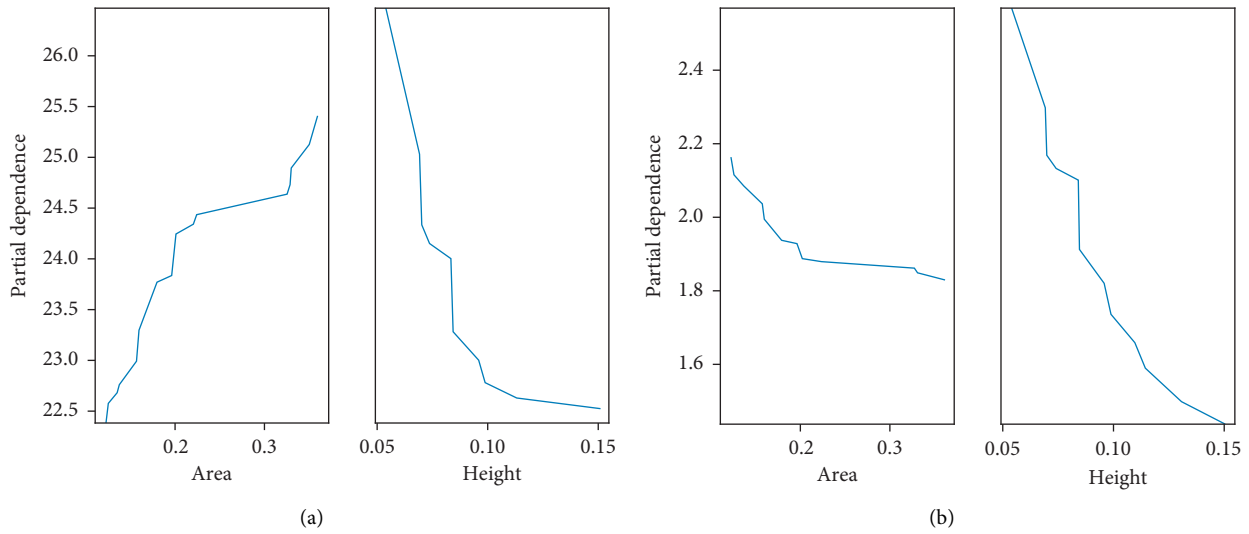

Figure 13: The partial dependence of sectional area (A) and bearing height (H) with (a) pier's top displacement and (b) bearing ESS.

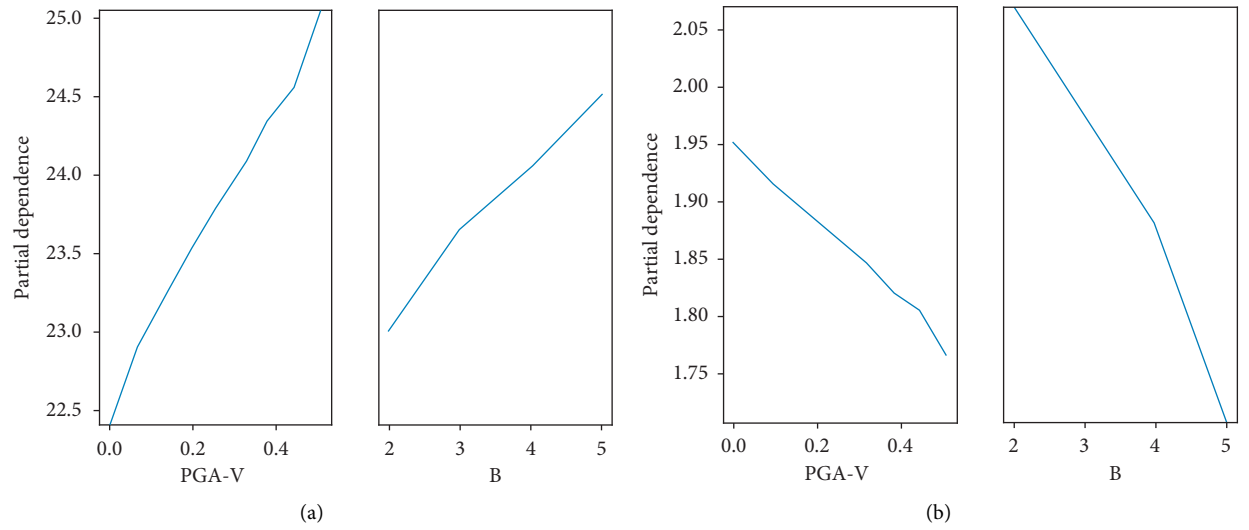

Figure 14: The partial dependence of vertical PGA (PGA-V) and bearing number (B) with (a) pier top displacement and (b) bearing ESS.

sectional area leads to the rise of the bearing stiffness, leading to the enhancement of the overall seismic response of the bridge. The bearing height (H) shows a significant negative correlation with the pier's seismic demands and bearing ESS. One explanation is that, on the one hand, because the increase of bearing height results in the decrease of the bearing stiffness, and it leads to the loss of the overall seismic response of the bridge, consequently reducing the pier' seismic demands. On the other hand, bearing ESS is inversely proportional to the bearing height, and the downward trend in Figure 13(b) confirms this correlation. Therefore, raising the height of bearing within an appropriate range can not only reduce the pier' seismic demands but also decrease the bearing ESS. The discovery of this phenomenon can provide a new thought for bridge seismic design.

Figure 14 shows the partial dependence relationship of seismic demands with the bearing's nongeometry parameters. The vertical seismic motion (PGA-V) is positively related to the pier' seismic demands and negatively associated with the bearing seismic demands. As the vertical seismic motion (PGA-V) increases, the bearing's friction coefficient reduces, and the bearing is more prone to sliding, so increasing indirectly the risk of hit between the beam and shear key, which increases the pier seismic demands in turn, the difference is about 11%. However, the vertical seismic motion (PGA-V) changing had less effect on the bearing seismic demands. Another interesting observation is that increasing the bearing number (B) will increase the pier seismic demands but decrease the bearing ESS. The reason is that the increasing the number of bearing (B) may change the stiffness distribution of the whole bridge, higher constraints in the transverse direction in a way, resulting in the higher seismic demands of the bridge. However, the seismic force shared by each bearing is reduced, leading to the decrease of bearing ESS. It is different from the conclusion of the traditional design method for bearing bridges.

By comparing the effects of vertical seismic strength (PGA-V), bearing number (B), sectional area (A), and bearing height (H) on bridge seismic demands, the factors sorted based on the value of the partial dependency function of pier seismic demands are as follows: $H > A >$ PGA-V $> B$, and the order of impact on the bearing ESS is $H > B > A >$ PGA-V. It can be concluded that the bearing height (H) is the most significant factor on the seismic demands of this type of bridge.

5. Conclusions

A series of tests confirmed the rules of laminated rubber bearings shear and sliding response on steel shims. Then, analytical models for the bearing and seismic demands model using the ANN were proposed. During the bridge seismic demands model, the influence of the various bearings design parameters was validated by partial dependency analysis. Moreover, the ANN bridge seismic demand model was applied to the bridge earthquake damage rapid assessment. The conclusions are as follows:

(1) The surface friction coefficients were found to increase with the increases in the vertical load by the performance test of LRB. The test data's correlation analysis determines that the bearing's critical characteristics are initial stiffness and friction coefficient. The geometric parameters were a vital factor to the initial stiffness of the bearing, and the friction coefficient is negatively related to the vertical load, which is different from the specified value of 0.2 of the coefficients of friction in Chinese specifications.

(2) By comparing the impact bearing design parameters to the seismic demands model, the order is sorted based on the value of the partial dependency function of pier seismic demands: $H > A >$ PGA-V $> B$, and the order of bearing factors to the bearing seismic demands is $H > B > A >$ PGA-V. The height of bearing is the most significant factor on the seismic demand model, which provides a new focus for the bridge seismic design.

(3) The seismic response of bridges varies greatly under different bearing models. The bearing response in the ANN model is larger than the MOTC model since the characteristics of the coefficient of friction with vertical load changes are accounted for. For the pier response, the result of the MOTC model is smaller than the ANN model when PGA $\leq$0.6 g, while PGA >0.6 g, the result of the MOTC model is far greater than the ANN model.

(4) The ANN method could be applied in the estimate of the seismic demand model with great performance after training. The results show that the R^2 of the bearing parameter and pier seismic demand in the ANN is 0.985, and the R^2 of the bearing seismic demand is 0.978 and with 98% accuracy of tag allocation, which means that the ANN method can complete the damage evaluation of seismic demands with high precision.

Data Availability

The nature of the data is the analytical data of the test and finite element models of the case bridge. The data used to support the findings of this study are available from the corresponding author upon request.

Conflicts of Interest

The authors declare that there are no conflicts of interest.

Acknowledgments

The research presented herein was supported by the Transportation Construction Science and Technology Project of Department of Transportation of Shanxi Province (2020-2-01), Science and Technology Project of Transportation Group of Shanxi Province (18-JKKJ-06, 18-JKKJ-07, and 19-JKKJ-11), and Transportation Construction Science and Technology Project of the Transportation Department of Inner Mongolia Autonomous Region (NJ-2020-17).

References

[1] J. S. Steelman, L. A. Fahnestock, J. F. Hajjar, and J. M. LaFave, "Cyclic experimental behavior of nonseismic elastomeric bearings with stiffened angle side retainer fuses for quasi-isolated seismic bridge response," *Journal of Bridge Engineering*, vol. 23, no. 1, pp. 1973–1987, 2018.

[2] J. S. Steelman, L. A. Fahnestock, E. T. Filipov, J. M. Lafave, J. F. Hajjar, and D. A. Foutch, "Shear and friction response of nonseismic laminated elastomeric bridge bearings subject to seismic demands," *Journal of Bridge Engineering*, vol. 18, no. 7, pp. 612–623, 2013.

[3] Q. Han, X. Du, J. Liu, Z. Li, L. Li, and J. Zhao, "Seismic damage of highway bridges during the 2008 Wenchuan earthquake," *Earthquake Engineering and Engineering Vibration*, vol. 8, no. 2, pp. 263–273, 2009.

[4] J. Li, T. Peng, and Y. Xu, "Damage investigation of girder bridges under the Wenchuan earthquake and corresponding seismic design recommendations," *Earthquake Engineering and Engineering Vibration*, vol. 7, no. 4, pp. 337–344, 2008.

[5] W. Zhuang and L. Chen, *Analysis of Highways' Damage in the Wenchuan Earthquake*, China Communications Press, Beijing, China, (in Chinese), 2013.

[6] C.-H. Lu, K.-Y. Liu, and K.-C. Chang, "Seismic performance of bridges with rubber bearings: lessons learnt from the 1999 Chi-Chi Taiwan earthquake," *Journal of the Chinese Institute of Engineers*, vol. 34, no. 7, pp. 889–904, 2011.

[7] ASTM D4014-03, *Standard Specification for Plain and Steel-Laminated Elastomeric Bearings for Bridges*, West Conshohocken, PA, USA, 2007.

[8] AASHTO M251-06, *Standard Specification for Plain and Laminated Elastomeric Bridge Bearings*, American Association of State Highway and Transportation Officials, Washington, DC, USA, 2008.

[9] JTG/T MOTC, *Specifications for Seismic Design of Highway Bridges*, China Ministry of Transportation and Communications Press, Beijing, China, (in Chinese), 2020.

[10] JTG/T MOTC, *Laminated Bearing for Highway Bridge*, China Ministry of Transportation and Communications Press, Beijing, China, (in Chinese), 2019.

[11] E. T. Filipov, J. R. Revell, L. A. Fahnestock et al., "Seismic performance of highway bridges with fusing bearing components for quasi-isolation," *Earthquake Engineering and Structural Dynamics*, vol. 42, no. 9, pp. 1375–1394, 2013.

[12] E. T. Filipov, L. A. Fahnestock, J. S. Steelman, J. F. Hajjar, J. M. Lafave, and D. A. Foutch, "Evaluation of quasi-isolated seismic bridge behavior using nonlinear bearing models," *Engineering Structures*, vol. 49, pp. 168–181, 2013.

[13] P. Deng, Z. Gan, T. Hayashikawa, and T. Matsumoto, "Seismic response of highway viaducts equipped with lead-rubber bearings under low temperature," *Engineering Structures*, vol. 209, pp. 8–25, 2020.

[14] A. M. Billah and B. Todorov, "Effects of subfreezing temperature on the seismic response of lead rubber bearing isolated bridge," *Soil Dynamics and Earthquake Engineering*, vol. 126, pp. 814–827, 2019.

[15] S. A. Mitoulis, "Uplift of elastomeric bearings in isolated bridges subjected to longitudinal seismic excitations," *Structure and Infrastructure Engineering*, vol. 11, No. 12, pp. 1600–1615, 2015.

[16] K. Kalfas, S. A. Mitoulis, and D. Konstantinidis, "Influence of steel reinforcement on the performance of elastomeric bearings," *ASCE Journal of Structural Engineering*, vol. 146, Article ID 04020195, 2020.

[17] N. Xiang and J. Li, "Experimental and numerical study on seismic sliding mechanism of laminated-rubber bearings," *Engineering Structures*, vol. 141, pp. 159–174, 2017.

[18] G. Wu, K. Wang, G. Lu, and P. Zhang, "An experimental investigation of unbonded laminated elastomeric bearings and the seismic evaluations of highway bridges with tested bearing components," *Shock and Vibration*, vol. 2018, Article ID 8439321, 18 pages, 2018.

[19] A. R. Bhuiyan and M. S. Alam, "Seismic performance assessment of highway bridges equipped with superelastic shape memory alloy-based laminated rubber isolation bearing," *Engineering Structures*, vol. 49, pp. 396–407, 2013.

[20] J. Ghosh, J. E. Padgett, and L. Dueñas-Osorio, "Surrogate modeling and failure surface visualization for efficient seismic vulnerability assessment of highway bridges," *Probabilistic Engineering Mechanics*, vol. 34, pp. 189–199, 2013.

[21] J. Guo, M. S. Alam, J. Wang, S. Shuai, and W. Yuan, "Optimal intensity measures for probabilistic seismic demand models of a cable-stayed bridge based on generalized linear regression models," *Soil Dynamics and Earthquake Engineering*, vol. 131, pp. 1–14, 2020.

[22] H. Jia, J. Lin, and J. Liu, "Bridge seismic damage assessment model applying artificial neural networks and the random forest algorithm," *Advances in Civil Engineering*, vol. 2020, Article ID 6548682, 13 pages, 2020.

[23] S. Hwang, S. Mangalathu, J. Shin, and J. S. Jeon, "Machine learning-based approaches for seismic demand and collapse of ductile reinforced concrete building frames," *Journal of Building Engineering*, vol. 34, Article ID 101905, 2020.

[24] J. Kiani, C. Camp, and S. Pezeshk, "On the application of machine learning techniques to derive seismic fragility curves," *Computers and Structures*, vol. 3, pp. 4–19, 2019.

[25] E. Figueiredo, I. Moldovan, A. Santos, P. Campos, C. João, and W. A. Costa, "Finite element–based machine-learning approach to detect damage in bridges under operational and environmental variations," *Journal of Bridge Engineering*, vol. 27, no. 7, Article ID 04019061, 2019.

[26] K. Wang, *Seismic Research of Bridge*, China Railway Publishing House, Beijing, China, (in Chinese), 2nd edition, 2014.

[27] K. Wang, G. Lu, and P. Zhang, "Study on seismic design methods for highway medium-span and small-span girder bridges based on machine learning," *Journal of Highway and Transportation Research and Development*, vol. 36, no. 2, pp. 74–84, 2019, (in Chinese).

[28] G.-Y. Lu, K.-H. Wang, and P.-P. Zhang, "Seismic design and evaluation methods for small-to-medium span highway girder bridges based on machine learning and earthquake damage experience," *Journal of Highway and Transportation Research and Development (English Edition)*, vol. 13, no. 1, pp. 24–37, 2019, (in Chinese).

[29] A. A. H. Alwanas, A. A. Al-Musawi, S. Q. Salih, H. Tao, M. Yaseen, and Z. M. Yaseene, "Load-carrying capacity and mode failure simulation of beam-column joint connection: application of self-tuning machine learning model," *Engineering Structures*, vol. 194, pp. 220–229, 2019.

[30] G. Wu, K. Wang, P. Zhang, and G. Lu, "Effect of mechanical degradation of laminated elastomeric bearings and shear keys upon seismic behaviors of small-to-medium-span highway bridges in transverse direction," *Earthquake Engineering and Engineering Vibration*, vol. 17, no. 1, pp. 205–220, 2018.

[31] C. Li, "Performance based seismic design of small and medium span girder bridges," Doctoral. Thesis, Southeast University Nanjing, Jiangsu, China, 2015.

[32] Z. Li, F. Ge, and X. Xu, "Finite element simulation and experimental study of property for elastomeric pad bearing," *Journal of Southeast University*, vol. 42, pp. 1299–1305, 2013, (in Chinese).

[33] D. Konstantinidis, J. M. Kelly, and N. Makris, *Experimental Investigation on the Seismic Response of Bridge Bearings," Tech. Rep., Pacific Earthquake Engineering Research Center*, University of California, Berkeley, CA, USA, 2008.

[34] J. S. Steelman, "Sacrificial bearing components for quasi-isolated response of bridges subject to high-magnitude, Low-Probability Seismic Hazard," [Doctoral. thesis], University of Illinois at Urbana-Champaign, Champaign, IL, USA, 2013.

[35] X. Huang, "Experimental and Theoretical Research on Unseating-Prevention Device for Continuous Bridges," Doctoral. Thesis, Tongji University, Shanghai, China, 2009.

[36] Y. Fang, "Research on typical damage of simple supported beam bridge during Wenchuan earthquake and transverse retainer device," Doctoral. Thesis, Tongji University, Shanghai, China, 2012.

[37] D. C. Kent, "Inelastic behavior of reinforced concrete members with cyclic loading," Doctoral. Thesis, University of Canterbury, Christchurch, New Zealand, 1969.

[38] F. C. Filippou, E. P. Popov, and V. V. Bertero, "Effects of bond deterioration on hysteretic behavior of reinforced concrete joints," *Tech. Rep., Pacific Earthquake Engineering Research Center*, University of California, Berkeley, CA, USA, 1983.

[39] L. Xu and J. Li, "Design and experimental investigation of a new type sliding retainer and its efficacy in seismic fortification," *Engineering Mechanics*, vol. 33, no. 2, pp. 111–118, 2016, (in Chinese).

[40] S. Akkar, M. A. Sandikkaya, and B. O. Ay, "Compatible ground-motion prediction equations for damping scaling factors and vertical-to-horizontal spectral amplitude ratios for the broader Europe region," *Bulletin of Earthquake Engineering*, vol. 12, no. 1, pp. 517–547, 2014.

[41] R. L. Iman and W. J. Conover, "Small sample sensitivity analysis techniques for computer models.with an application to risk assessment," *Communications in Statistics - Theory and Methods*, vol. 9, no. 17, pp. 1749–1842, 1980.

[42] S. Mangalathu, J.-S. Jeon, J. E. Padgett, and R. DesRoches, "Performance-based grouping methods of bridge classes for regional seismic risk assessment: application of ANOVA, ANCOVA, and non-parametric approaches," *Earthquake Engineering & Structural Dynamics*, vol. 46, no. 14, pp. 2587–2602, 2017.